The Effect of Selectivity Enhancers on the Structure of Palladium during High-Pressure Continuous-Flow Direct Synthesis of Hydrogen Peroxide in Ethanol

Benedikt J. Deschner[a], Dmitry E. Doronkin[b,c]*, Thomas L. Sheppard[b,c], Anna Zimina[b,c], Jan-Dierk Grunwaldt[b,c], Roland Dittmeyer[a,b]*

[a]Institute for Micro Process Engineering, KIT, Hermann-von-Helmholtz-Platz 1, Eggenstein-Leopoldshafen, 76344, Germany

[b]Institute of Catalysis Research and Technology, KIT, Hermann-von-Helmholtz-Platz 1, Eggenstein-Leopoldshafen, 76344, Germany

[c]Institute for Chemical Technology and Polymer Chemistry, KIT, Engesserstr. 20, Karlsruhe, 76131, Germany

KEYWORDS. H_2O_2, direct synthesis, X-ray absorption spectroscopy, Pd, hydride, in situ, operando

ABSTRACT: A potentially green process to produce hydrogen peroxide (H_2O_2) is its direct synthesis from molecular hydrogen and oxygen. Still, the lack of mechanistic understanding of the reaction impedes a knowledge-based catalyst design for improved selectivity and stability. In this study, we employed X-ray absorption spectroscopy (XAS) to obtain structural information on a titania-supported palladium (Pd) catalyst under H_2O_2 synthesis conditions. The study focuses on the effect of the liquid-phase H_2:O_2 ratio between 0.67 and 3 and solvent composition under industrially relevant conditions, that is ethanol with and without H_2SO_4 and NaBr as selectivity enhancers at 40 bar. The X-ray near-edge structure of the absorption spectra (XANES) and the extended X-ray absorption fine structure (EXAFS) revealed that ethanol fully reduces Pd nanoparticles, even when saturated with oxygen. Oxygen presence at the Pd surface could only be suspected based on its small contribution to the EXAFS signal. A palladium hydride phase is detected under stoichiometric conditions due to lattice expansion. Addition of H_2SO_4 causes Pd lattice expansion and an increased yield at stoichiometric conditions. Further addition of bromide did not lead to any significant change in catalyst state and activity.

Introduction

Hydrogen peroxide (H_2O_2) constitutes an efficient and versatile liquid commodity oxidant with large-scale applications ranging from bleaching pulp and paper to semiconductor etching [1]. Cheap H_2O_2 offers the potential to pave the way to a cleaner and more sustainable industrial oxidation chemistry [2] as it generates only water as by-product in contrast to chlorinated oxidizers. Despite its advantages, H_2O_2 is still not economically competitive compared to other oxidizers [3] which is related to the anthraquinone process [4], the current standard for industrial H_2O_2 production. This process comprises a complex multi-stage process which is only economical in large-scale plants [5].

The centralized production, however, requires shipping concentrated solutions [6] and thus these expenses antagonize a further H_2O_2 price reduction. The appeal of small-scale on-site production for cheap H_2O_2 has fueled the search for process alternatives in the last decade [1,3,7], such as electrochemical synthesis [8–11], plasma processes [12,13] and the direct synthesis of H_2O_2 [14–16].

The direct synthesis of H_2O_2 is an attractive route that involves reacting both molecular hydrogen and oxygen over a palladium-based supported catalyst in contact with a liquid phase in a single process stage [17]. The process so far has only entered the pilot phase [18] . The main reason impeding a viable process is the low selectivity [19]. This results from parallel and consecutive H_2O formation (Scheme 1) associated with irreversible O-O bond scission [20]. Therefore, the key for commercialization is kinetic control for high selectivity in conjunction with a high structural stability, even at high H_2O_2 concentrations in the reaction mediumKlicken oder tippen Sie hier, um Text einzugeben.. This challenge calls for a rational catalyst design based on a fundamental understanding of the reaction. Although many different key findings have been disclosed on the mechanism, however, a consistent picture of direct synthesis has not yet been established at the molecular level [14,17].

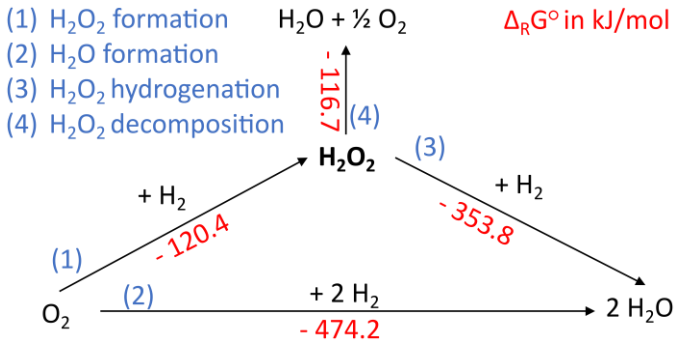

Scheme 1. Reaction network of the direct synthesis of H_2O_2.

In particular, the Langmuir-Hinshelwood-Hougen-Watson (LHHW) model is the most widely assumed mechanism [21–24] where surface-activated hydrogen species react with absorbed dioxygen adsorbed on the catalyst surface. However, the LHHW model was inconsistent with the recent experimental results of Wilson and Flaherty [25]. Instead, the authors proposed a heterolytic mechanism characterized by a proton-electron transfer where H_2O_2 is formed from two-electron oxygen reduction (ORR) with solvent protons and electrons released by hydrogen oxidation reaction (HOR) without external electric circuit. The mechanism is supported by experimental similarities to the electrocatalytic oxygen reduction reaction [26]. Moreover, recent results propose that hydrogen in the form of a metal hydride may also contribute to the reaction [27,28]. This illustrates that the electronic state of hydrogen is still insufficiently understood.

Likewise, there are different views on the mode of interaction of the solvent additives bromide and mineral acids denoted as "selectivity enhancers" [16,17,29]. Bromide has been attributed to promote the selectivity through site blocking [30–32], nanoparticle restructuring [29], but also electronic effects, i.e. reducing the occupation of the electronic levels near the Fermi level to diminish the O-O cleavage reactivity [14]. Brønsted acids have been attributed to diminish the base-catalyzed decomposition of H_2O_2 [16] and also to electronically modify the surface[33], in particular supporting the oxidation of the palladium nanoparticles in order to inhibit the sites responsible for water formation [29]. Since both bromide and acids have been ascribed an electronic effect, the question inevitably arises as to how the selectivity promoters and the solvent itself influence the electronic state of the catalyst, which in turn could provide insights into the actual mechanism. However, the matter is even more complicated because it is known that the oxidation state of palladium can vary depending on the hydrogen and oxygen concentrations within a single reactor [27,34,35]. In this light,

experimental studies uncovering structure-activity relationships under actual working conditions are one important element to get closer to mechanistic understanding on a molecular level.

X-ray absorption spectroscopy (XAS) is a powerful method that enables nondestructive structural characterization of catalysts under working conditions [36], revealing the metal oxidation state and coordination environment amongst other key data [37]. The direct synthesis has so far only been investigated in a few studies using XAS *operando* or *in situ* [27,38–42], because it is challenging to safely operate this three-phase reaction under increased pressure and simultaneously perform X-ray measurements at a synchrotron facility. However, these conditions are necessary to obtain structure-performance relationships in the actual relevant process window. In this XAS study, we present the structural changes of supported monometallic palladium nanoparticles in true continuous-flow of ethanoic media at 40 bar corresponding to industrially relevant working conditions [43,44]. With defined stepping the H_2:O_2 ratio from 2:3 to 3:1, we first elucidate the palladium nanoparticle structure in pure ethanol. We further analyze the effects of H_2SO_4 and NaBr in ethanol in both oxygen and hydrogen-rich conditions, and compare the resulting structure-activity relationships with the data obtained in water medium [27].

Methods

Catalyst preparation and methods

We used a titania-supported palladium catalyst as described in our previous operando XAS study [27]. The catalyst was synthesized by wet-impregnation according to the procedure described by Inoue et al. [45]. Briefly, 10 g of rutile phase titania powder (Nanostructured & Amorphous Materials Inc., 50 nm average particle size, 99.9%) was immersed under vigorous stirring into 100 mL

aqueous solution HCl (Merck, 1.0M) and 167 mg $PdCl_2$ (Sigma-Aldrich, 99%). The resulting slurry was dried over a hot plate. The solid was gently ground into a fine powder, which was subsequently calcined in static air for 6 h at 350°C, then reduced in a flow of 5%H_2/95%Ar for 3 h at 350°C. We obtained 50–200 µm agglomerates for use in the continuous-flow cell by uniaxial pressing and sieving. The final metal content of Pd was 1 wt.-%, confirmed by ICP-OES (Agilent 725). The average Pd nanoparticle (NP) size was 2.8 nm according to transmission electron microscopy (FEI Titan 80-300) [27].

High Pressure Setup and Experimental Procedure

The setup is based on the process concept of spatial separation of gas-liquid mass transport and catalytic reaction, resulting in a single-phase liquid flow with dissolved gases through the fixed bed (Scheme 2). A defined gas flow of synthetic air or hydrogen respectively (controlled by mass flow controllers) is mixed with a defined volume flow of solvent (controlled by HPLC pumps). The gases are then continuously dissolved in the liquid for bubble-free single-phase flow by means of SiC packed beds for enhanced interfacial mass transfer. The entire experimental setup except for the HPLC pump heads was thoroughly degreased and *in situ* passivated according to a standard nitric acid procedure [46] so that the H_2O_2 decomposition is estimated to be less than 5% with respect to the concentration immediately after the XAS cell (cf. Supporting Information S2). The catalytic cell with PEEK X-ray windows (2 mm thickness) was loaded with impregnated 1%Pd/TiO_2 catalyst, (sieve fraction 50–200 µm). Sample loading was 35 ± 5 mg with a sample volume of ca. 12 x 5 x 1 mm (length x depth x width). The catalyst was packed in between two quartz wool plugs, which were supported by a 6–8 mm long bed of SiC particles (sieve fraction 50–200 µm,

Alfa Aesar), in turn, supported by further quartz wool plugs for enhanced packed-bed stability. The liquid stream flowing out of the reactor was monitored using a near-infrared (NIR) spectrometer (multispec® NIR, tec5) coupled to a high-pressure transmission process flow cell (3/8″ Process Flow Cell, Ocean Optics).

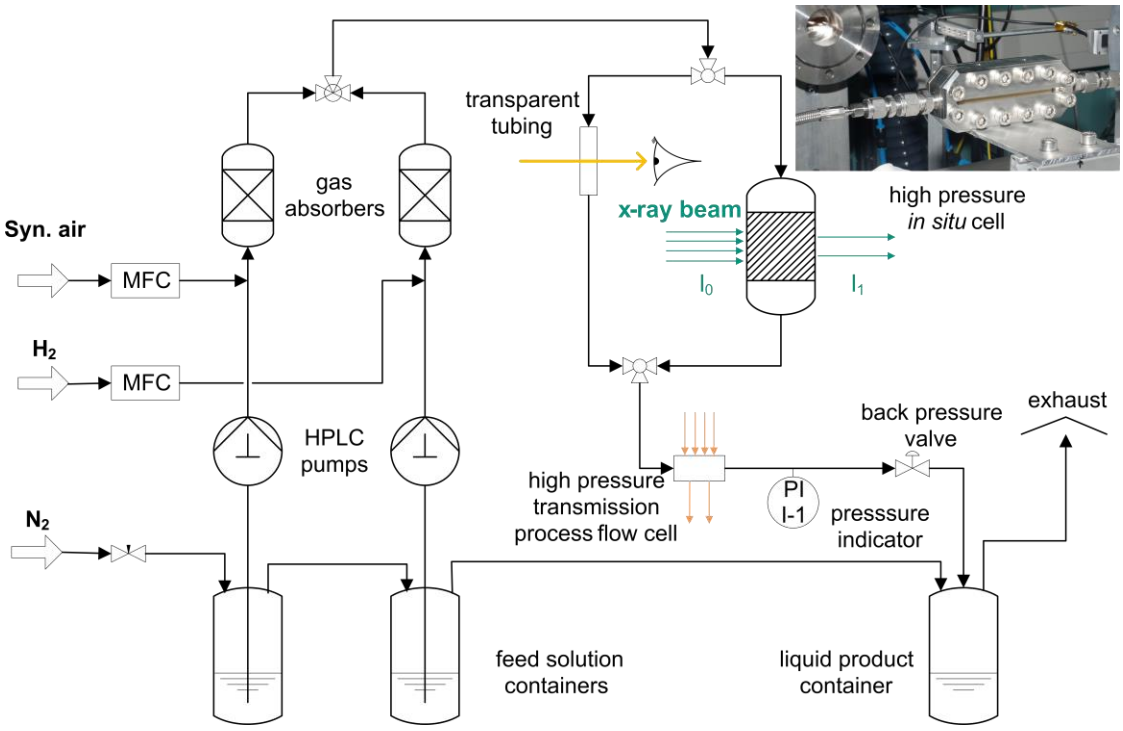

Scheme 2. High-pressure continuous-flow setup.

All experiments were conducted at 40 bar system pressure for complete gas dissolution upstream of the XAS cell and at ambient temperature. The first measurement series aimed at investigating the influence of different H_2:O_2 ratios in ethanol solution. Therefore, a constant flow (rate: 3.0 mL_{NTP}/min) of pure hydrogen (5.0 purity, Alphagaz^{TM} 1, Air Liquide) was dissolved in a

constant liquid flow (rate: 1.0 mL/min) of absolute ethanol (≥ 99.8% E, ACS, AnalaR NORMAPUR®, VWR BDH Chemicals) and subsequently mixed with another constant stream of absolute ethanol (rate: 7.18 mL/min) and varying flow of synthetic air. Thus, the combined liquid flow was set to 8.18 ml/min resulting in a low catalyst contact time (τ_{mod} = 2.4 ± 0.5 (kg_{Pd} s)/m^3) with a fixed hydrogen concentration of 16.4 mmol/L, corresponding to a thermodynamic saturation pressure of 4.8 bar according to ref [47]. Oxygen was added as synthetic air (20.9±0.2% O_2 in N_2, 5.0 purity, Alphagaz™ 2, Air Liquide) with air (oxygen) gas flows between 4.8 (1.0) mL/min and 28.7 (6.0) mL/min to fit the range of the available mass flow controller. Complete dissolution of gases was confirmed when no bubbles could be observed for at least 45 min through the piece of transparent tubing in the bypass channel of the setup (Scheme 2). To obtain reference spectra, ethanol streams containing only synthetic air or H_2, respectively, were fed to the catalytic fixed bed. Table 1 shows the experimental conditions with gradually increased hydrogen content, starting from oxygen towards hydrogen only. The measurements were done in total on three catalyst beds, the catalyst bed replacement was required due to poor mechanical stability of the used catalyst which resulted in blocking of the flow through the reactor. After each repacking of the reactor the catalyst was reduced in flow of pure ethanol for a minimum of 5-8 hours (until no changes in the Pd XANES spectra were observed). At first, the reference conditions (O_2 only and H_2 only) were measured. The following measurements (reactor repacked with a new catalyst bed) were intended to cover the most different conditions with respect to the reducing potential, finally (new catalyst bed) approaching stoichiometric H_2:O_2 ratio, and at last probing the influence of selectivity enhancers.

Table 1. Reaction conditions with pure ethanol as reaction solvent. Gas flow at standard reference according to DIN 1343[48] (T° = 273.15 K, p° = 1013.25 hPa).

No.	H_2:O_2 ratio (-)	H_2 gas flow (mL/min)	Ethanol flow (H_2 channel) (mL/min)	Air (O_2) gas flow (mL/min)	Ethanol flow (O_2 channel) (mL/min)
1	O_2 only	0	1.0	28.70 (6.0)	7.18
2	0.67	3.0	1.0	21.50 (4.5)	7.18
3	1	3.0	1.0	14.35 (3.0)	7.18
4	1.5	3.0	1.0	9.57 (2.0)	7.18
5	2	3.0	1.0	7.17 (1.5)	7.18
6	2.4	3.0	1.0	5.98 (1.25)	7.18
7	3	3.0	1.0	4.80 (1.0)	7.18
8	H_2 only	3.0	1.0	0	7.18

[a] [H_2 concentration]/[O_2 concentration] in ethanol, calculated as [H_2 gas flow]/[O_2 gas flow] (steady-state complete gas dissolution).

The second measurement series aimed at investigating the influence of adding sulfuric acid and sodium bromide. We studied the Pd/TiO_2 catalyst in absolute ethanol containing 0.12 mol/L sulfuric acid (95–97%, p.a, EMSURE® ISO, Merck) at a fixed H_2:O_2 ratio of 0.67 in a combined ethanoic solution flow of 8.18 mL/min. Subsequently, the solvent was further modified through adding solid sodium bromide (purum p.a., Fluka). For this reason, 314 mg of NaBr was added to 2.1 L of the previously prepared ethanol with 0.12 mol/L sulfuric acid and stirred for 30 min. After that, the remaining solid residue was removed by filtration. Solubility of NaBr in pure ethanol is reported as approx. 2.5 g per 100 g solvent [49], and Na_2SO_4 is practically insoluble [50]. After drying in ambient air, the weight of the solid residue (a mixture of NaBr and $Na_2SO_4 \cdot 10H_2O$) was determined as 316 mg. From the mass change a bromide concentration of approx. 0.02 mmol/L was estimated. The influence of acidic and bromide additives was studied at fixed H_2:O_2 ratios of 0.67 and 2 in the combined liquid flow of 8.18 mL/min.

Safety note: The experiment features potential explosive hazard, as oxidizing synthetic air is combined with the fuels H_2 and ethanol at elevated pressure. A dry-out of the catalyst in presence of a H_2/O_2 gas mixture is critical in particular, as this is known to ignite [51]. Hence, bubble-free saturation via inline absorption columns is crucial for safe operation which requires extensive testing prior to reaction experiments. The process conditions require pressure-rated equipment; devices in O_2-enriched atmosphere must be specially cleaned and free of grease. Further safety measures include narrow restriction of the process window (automatic mass flow controller shutdown in case of high flow of reactant gases, high-pressure pump shutdown), small diameter tubes for minimized liquid holdup, and electrical grounding of the tubing. The reactor effluent container is N_2-purged to ensure H_2 concentrations in the effluent below its lower explosive limit.

Note on mass transfer limitations: The absence of external and internal mass transport limitations is crucial for the significance of the X-ray absorption spectroscopy itself as this technique provides volume-averaged structural information of the catalyst sample. The Weisz-Prater criterion[52] indicates that the catalyst was operated at the limit with respect to internal (pore diffusion) mass transport limitations in this study (Supporting Information S3). The Mears criterion [53] confirms that no mass transport limitations are anticipated due to high flow rate of 8.18 mL/min (Supporting Information S4).

Determination of the H_2O_2 concentration

Catalytic performance during XAS experiments was qualitatively monitored by a NIR spectrometer probing the liquid stream at the outlet of the reactor (cf. Supporting Information S5), however due to overlapping H_2O_2 and H_2O absorbance bands activity and selectivity could not be

quantitatively analyzed using the NIR spectra measured at the beamline. The H_2O_2 concentration was determined by repeating the experiments in the laboratory using the same experimental setup and identical conditions to the synchrotron studies but complete sodium bromide dissolution (5 mmol/L NaBr). The amount of produced H_2O_2 was determined manually by cerimetric redox titration by repeating the experimental procedure in the laboratory. For the titration, 50 µL ferroin indicator solution were added to 50 mL of diluted sulfuric acid (1:19 vol. H_2SO_4/H_2O). The stirred solution was titrated with 0.01 M $Ce(SO_4)_2$ (approx. 125 µL) until a color change from red to pale blue was observed. 10 mL of the product solution were added and titrated with 0.01 M $Ce(SO_4)_2$ to a pale blue endpoint. The measurement uncertainty equals 0.05 mmol/L corresponding to the pipette volume of 10 µL used for the titration.

We note that quantifying the H_2 and O_2 concentrations the effluent concentration may be sufficient to obtain the moles of reactants consumed as the mass flow controllers define the molar flow to the reactor. Quantifying the H_2 and O_2 concentrations is possible using Raman spectroscopy or gas analysis (e.g. gas chromatography with thermal conductivity detector or mass spectrometry) in the effluent but was not followed in this study because this is very demanding in terms of instrumentation. Instead, a simpler titration method was used to monitor the H_2O_2 concentration in the laboratory experiments.

X-ray Absorption Spectroscopy and Data Analysis

XAS measurements at the Pd K absorption edge were performed at the CAT-ACT beamline (CAT experimental station) at the KIT synchrotron radiation source [54] using a 2.5 T wiggler source (40 poles, 48 mm period length) and a DCM with a Si (311) crystal pair. The beam size was 0.6 mm (vertical) x 2 mm (horizontal). The experiments were performed in transmission geometry using

ionization chambers as detectors. Spectra were measured at the beginning and end of the catalyst bed. The spectra were normalized and the extended X-ray absorption fine structure (EXAFS) spectra background subtracted using the ATHENA program from the IFFEFIT software package.[55] The k^1-, k^2-, and k^3-weighted EXAFS functions were Fourier transformed (FT) in the k range of 2.5–10.5 $Å^{-1}$ and multiplied by a Hanning window with sill size of 1 $Å^{-1}$. The FT EXAFS spectra are shown without phase shift correction. The structural model was based on a Pd metal core (ICSD collection code 52251) and (for a spectrum in O_2-saturated ethanol) a Pd-O first shell modeled using PdO (ICSD collection code 24692). The structure refinement was performed using the ARTEMIS software (IFFEFIT).[55] For this purpose the corresponding theoretical backscattering amplitudes and phases were calculated by FEFF 6.0.[37] The theoretical data were then adjusted to the experimental spectra by a least square method in R-space between 1 and 3 Å. First, the amplitude reduction factor (S_0^2 = 0.87) was calculated using the Pd foil reference spectrum and then the coordination numbers, interatomic distances, energy shift (δE_0) and mean square deviation of interatomic distances (σ^2) were refined. The absolute misfit between theory and experiment was expressed by ρ.

Results and Discussion

Structure of Pd species during direct synthesis of H_2O_2 in pure ethanol

Reference conditions

After the initiation of the oxygen dosage for single-phase flow of dissolved oxygen in pure ethanol (condition 1, Table 1), the XANES signature gradually changed from partially oxidized state [27] and was stable after 5 hours on stream showing fully reduced palladium (Figure 1a). EXAFS shows

a Pd-Pd distance identical to the Pd reference (Figure 1b). The complete reduction of Pd shown here even in O_2-saturated feed is exceptionally different from the behavior in oxygen-saturated water containing bromide observed in our previous study using the same catalyst. In water, the Pd NPs were found to be decorated with chemisorbed oxygen showing an oxidic Pd^{2+} fraction up to 20% [27]. Sweeping the catalyst with single-phase flow of dissolved hydrogen in pure ethanol resulted in a PdH_x signature, both in XANES and EXAFS. In XANES, a shift of a peak at 24387 eV towards lower energies was observed [27,56]. In EXAFS, a lateral peak shift towards higher Pd-Pd bond distances was observed in line with lattice expansion due to interstitial hydrogen [57,58].

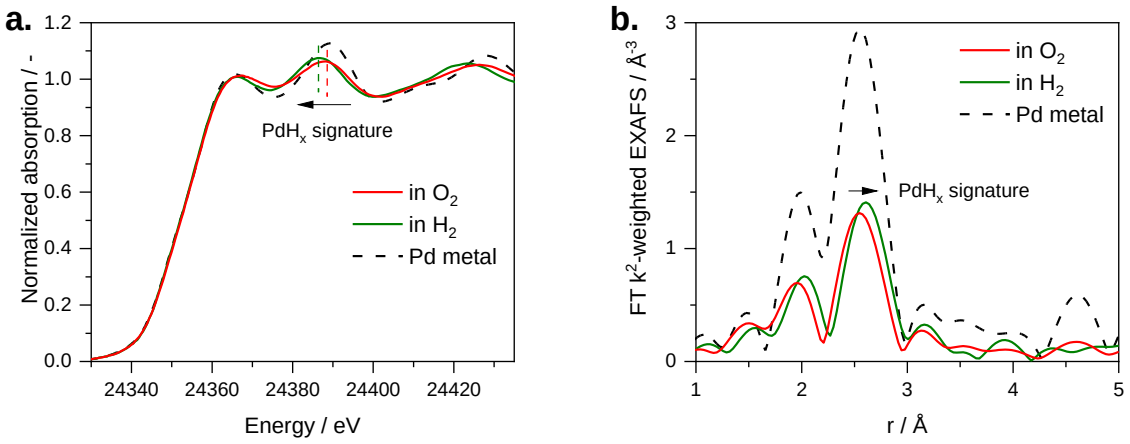

Figure 1. Pd-K edge (a) XANES and (b) Fourier transformed (FT) EXAFS spectra of the Pd/TiO_2 catalyst under reference conditions (O_2- and H_2-saturated ethanol) compared to the spectrum of metallic Pd. k^2-weighted EXAFS spectra are given in Figure S6a in order to allow evaluating the data quality at ambient temperature in ethanol.

Working conditions

The H_2:O_2 ratio was adjusted to the desired values (Table 1) and XAS spectra were recorded after the XANES region of the spectrum was found not to change, which typically occurred after at least 1 hour time on stream. Spectra measured under working conditions near the beginning and end of the catalyst bed were generally similar. This behavior shows that the catalyst state over the entire length of the bed was uniform, verifying the aspired differential operation mode of the packed bed reactor. For this reason, the spectra measured near the end of the catalyst bed are reported due to generally better quality, with the exception of an experiment at H_2:O_2 = 1, where only the beginning was probed. The better data quality is associated with the fact that displacement or compaction of the catalyst bed (i.e. mechanical stability issues) have less effect on the end position of the catalyst bed (higher packing density and no pinholes). The full set of XANES spectra recorded under working conditions exhibits only small variations in the whole range of tested H_2:O_2 ratios between oxygen-rich and hydrogen-rich conditions (Figure 2a). No sign of oxidized Pd could be identified in the XANES spectra under working conditions, neither in hydrogen-rich nor in oxygen-rich conditions. Thus, contrary to our findings using aqueous reaction medium[27], there is no substantial contribution from chemisorbed oxygen in the XANES data.

In the corresponding EXAFS spectra, the Pd peak position (between 2.5 and 3.0 Å) shifted towards larger distances and the backscattering intensity increased with higher partial pressure of hydrogen (Figure 2b). This is in line with previous studies in water [27]. A small contribution from a light atom, most probably O, may be present in the EXAFS spectra at approx. 1.8 Å, see Table S2 and Figure S7 in the SI for comparison of the fits with and without accounting for a light atom contribution. This contribution is more visible under oxygen excess and approaches zero (if uncertainty/error bars are taken into account) with more hydrogen. Compared to the previous study in water [27], very small amounts of oxygen still may be chemisorbed on the Pd NPs but they do not

change the electronic state of Pd (e.g. oxidation) or this change is countered by interaction with ethanol so that the XANES spectral region is not influenced. Since this contribution is very minor and often within error bars, in the following only the first Pd-Pd shell was fitted.

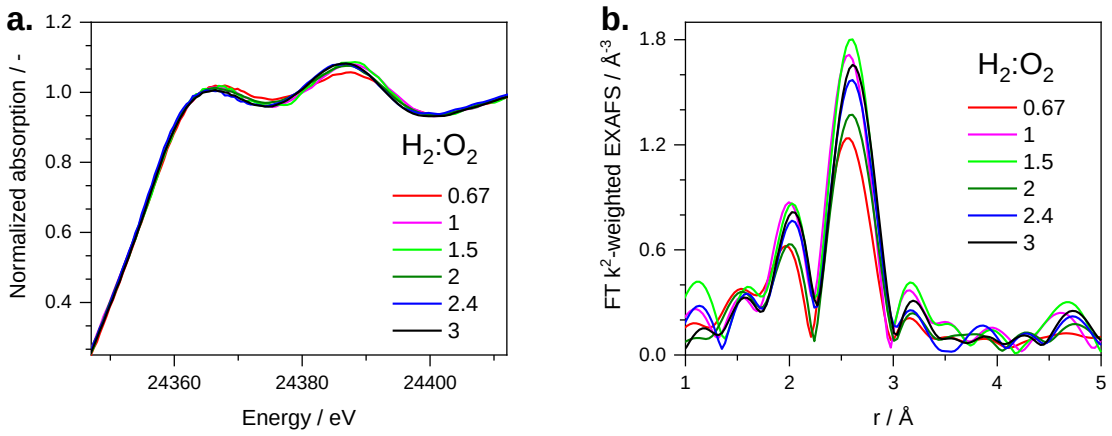

Figure 2. Pd-K edge (a) XANES and (b) FT EXAFS spectra of the Pd/TiO_2 catalyst under different H_2:O_2 ratios in the feed. For k^2-weighted EXAFS data in k-space see Figure S6b.

With increasing H_2:O_2 ratio, an elongation of the Pd-Pd interatomic distances was observed (Figure 3) and changes in Pd NP state from metallic Pd^0 to ß-PdH_x [27,56–58]. The observed interatomic distances under working conditions can be clustered into three groups: (1) Only small Pd lattice expansion (d(Pd-Pd) ≤ 2.76 Å) at H_2:O_2 = 0.67 and 1 is observed, possibly, α-PdH_x [56]. (2) Conditions 2.4 and 3 correspond to the structure observed with only hydrogen dissolved in ethanol solution (d(Pd-Pd) ≥ 2.80 Å), thus the formation of β-PdH_x [56]. (3) In between (d (Pd-Pd) between 2.76 and 2.80 Å), that is conditions 1.5 and 2, a plateau is observed within experimental error. This is in line with a mixed α+β phase composition which are observed for bulk Pd-H

sorption isotherms [56,59]. Compared to the previous study, this intermediate structure expansion is still well visible due to improved discrimination of concentration ratios and more data points, respectively. A shift of the XANES peak at approx. 24387 eV to lower energies with the increase in the H_2:O_2 ratio additionally confirms transformation from the metallic state to PdH_x (Figure 3, red circles) [27,56]. Furthermore, the reversible increase in the first shell coordination number under hydride-forming conditions has also been observed in the previous study in water [27] and attributed to hydrogen-induced transformation of Pd NPs from octahedral to icosahedral symmetry.

We note that the α/β miscibility gap (i.e. the two-phase region) corresponds to a H_2 pressure of about 20 mbar at room temperature in the thermodynamically equilibrated binary Pd-H system [60]. This is the case for bulk phase [61] as well as for nanoparticles, where the plateau has a positive slope and the two-phase region is smaller overall, but not shifted to lower pressures [62]. However, in our experiments we fed a constant H_2 concentration of 16.4 mmol/L corresponding to an H_2 pressure of 4.8 bar [61]. The α/β hydride phase transition observed at 4.8 bar H_2 (direct synthesis) instead of 20 mbar H_2 (binary Pd-H equilibrium) demonstrates that the direct synthesis alters the steady-state H surface coverage on the Pd NPs: the reaction itself determines the H concentration in the Pd bulk rather than the H_2 partial pressure over the catalyst as outlined by ref [63]. Consequently, the α/β hydride transition is kinetically controlled, suggesting a complex interaction between reaction kinetics and Pd hydride phase formation in the direct synthesis.

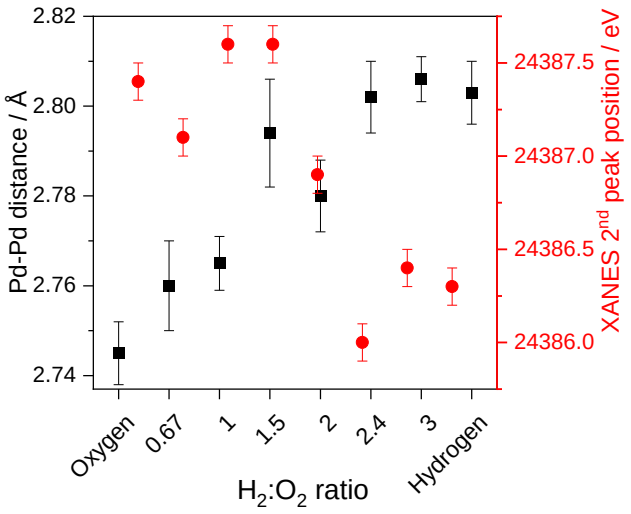

Figure 3. Average Pd-Pd distances obtained from EXAFS analysis (black squares) and position of the 2nd peak in the XANES spectra (red circles) depending on the H_2:O_2 ratio in pure ethanol.

Effect of promoters on the structure of Pd species

Addition of the mineral acid H_2SO_4 (alone and with NaBr) changed the catalyst state (Figure 4a,b). The analysis is reported in Table 3 (H_2:O_2 = 0.67) and Table 4 (H_2:O_2 = 2). Addition of H_2SO_4 at H_2:O_2 =0.67 causes stretching of the average Pd-Pd bond distance. This may mean more interstitial H in the Pd lattice. However, the change is relatively small and not visible when qualitatively comparing the positions of the Pd-Pd backscattering peaks at 2.6 Å (without phase shift correction, Figure 4b). Under hydrogen excess, addition of H_2SO_4+NaBr to ethanol results in strong features related to β-PdH_x in the XANES and EXAFS spectra (Figure 4c,d), the Pd-Pd distance is even longer than in the reference hydride spectrum (Table 2). Hence, addition of H_2SO_4 leads to

elongated Pd-Pd distances and the corresponding changes in XANES (Figure 5), possibly facilitating PdH_x formation.

Table 2. Refined structural parameters of the Pd/TiO_2 catalyst obtained from XANES analysis and EXAFS fitting during variation of H_2:O_2 ratio using pure ethanol as a solvent. Selected fits for the spectra measured in O_2- and H_2-saturated ethanol are given in Figure S8.

H_2:O_2 ratio →	**O_2 only**	**0.67**	**1**	**1.5**	**2**	**2.4**	**3**	**H_2**
$E_{max.}$ of 2nd peak in XANES (eV)	24387.4	24387.1	24387.6	24387.6	24386.9	24386.0	24386.4	24386.3
d Pd-Pd (Å)	2.745 ±0.007	2.760 ±0.010	2.765 ±0.006	2.794 ±0.012	2.780 ±0.008	2.802 ±0.008	2.806 ±0.005	2.803 ±0.007
CN Pd-Pd	9.0±1.0	9.5±1.4	9.5±1.1	10.2±2.5	10.5±1.1	10.6±1.3	11.0±1.0	10.2±1.0
σ^2 (10^{-3} Å^2)	9.7±1.1	10.1±0.8	7.7±1.0	7.7±2.0	10.7±1.1	9.2±1.1	9.0±0.8	9.8±1.0
δE_0 (eV)	-1.1±0.6	-1.3±1.0	-0.6±0.8	0.1±1.7	-0.8±0.7	-0.7±0.8	-0.3±0.6	-0.6±0.6
ρ (%)	1.0	1.7	0.8	1.1	0.9	0.7	0.7	0.8

Table 3. Refined structural parameters of the Pd/TiO_2 catalyst obtained from XANES analysis and EXAFS fitting at H_2:O_2 = 0.67 using pure ethanol or ethanol with H_2SO_4 and NaBr promoters. Values reported for spectra measured near both the beginning and end of the catalyst bed.

Conditions → **(position in catalyst bed)**	EtOH **(beginning)**	EtOH **(end)**	+H_2SO_4 **(beginning)**	+H_2SO_4 **(end)**	+H_2SO_4+ NaBr **(beginning)**	+H_2SO_4+ NaBr **(end)**
$E_{max.}$ of 2nd peak in XANES (eV)	24387.3	24387.1	24387.3	24387.3	24387.4	24386.8
d Pd-Pd (Å)	2.757±0.010	2.760±0.010	2.780±0.008	2.774±0.009	2.798±0.010	2.804±0.009
CN Pd-Pd	9.3±1.4	9.5±1.4	10.1±1.6	7.4±1.5	10.7±2.2	10.0±1.8
σ^2 (10^{-3} Å^2)	10.5±1.4	10.1±0.8	7.9±1.3	4.6±1.6	8.2±1.7	7.5±1.4
δE_0 (eV)	-1.5±1.0	-1.3±1.0	0.1±1.0	-0.8±1.3	0.6±1.2	-0.4±1.1
ρ (%)	1.8	1.7	0.9	1.7	1.3	1.1

Table 4. Refined structural parameters of the Pd/TiO_2 catalyst obtained from XANES analysis and EXAFS fitting at $H_2:O_2 = 2$ using pure ethanol or ethanol with H_2SO_4 and NaBr promoters. Values reported for spectra measured near the beginning of the catalyst bed.

Conditions → **(position in catalyst bed)**	EtOH **(beginning)**	$+H_2SO_4$+NaBr **(beginning)**
max. of peak B (eV)	24387.3	24386.3
d Pd-Pd (Å)	2.780±0.007	2.810±0.007
CN Pd-Pd	9.6±1.2	9.8±1.3
σ^2 (10^{-3} Å^2)	9.0±1.1	6.5±1.1
δE_0 (eV)	-1.0±0.8	-0.4±0.8
ρ (%)	1.0	1.0

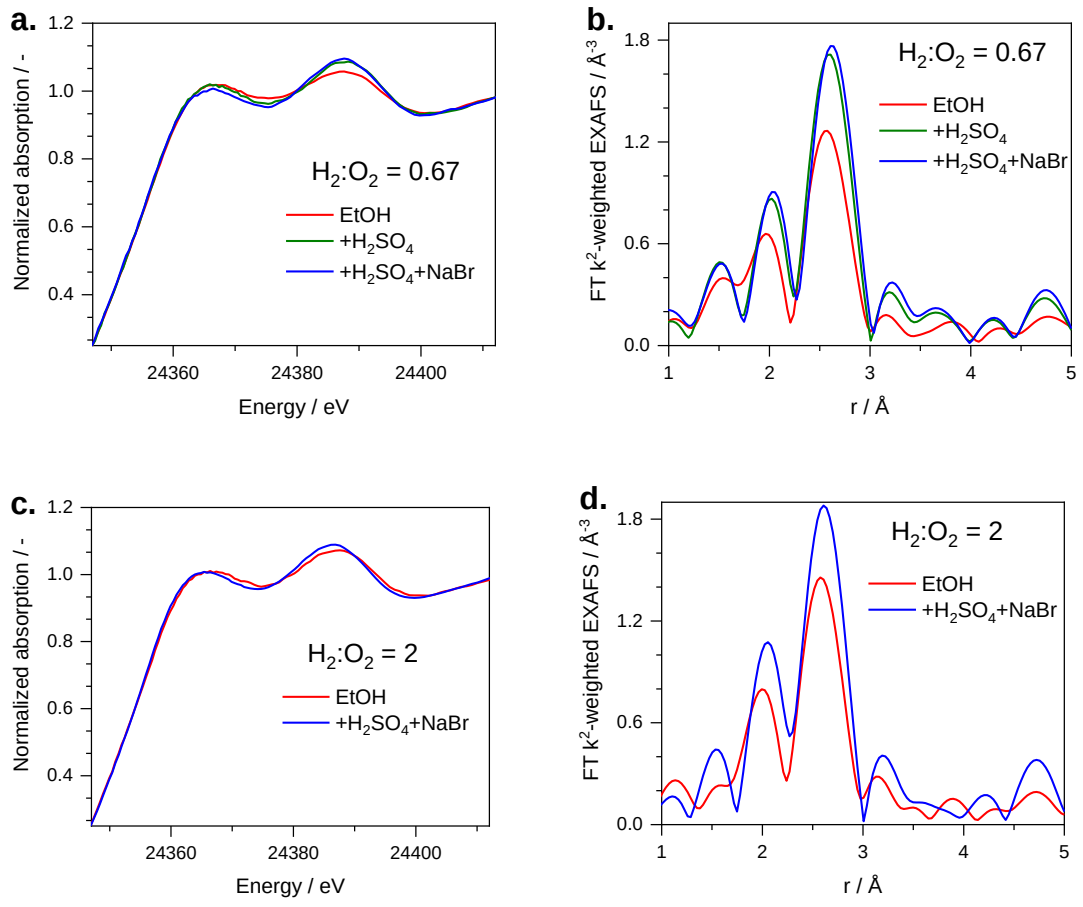

Figure 4. Pd-K edge (a) XANES and (b) FT EXAFS spectra of the Pd/TiO_2 catalyst under conditions of the direct H_2O_2 synthesis at (a., b.) $H_2:O_2 = 0.67$ and (c., d.) $H_2:O_2 = 2$. The spectra

were measured near the beginning of the catalyst bed. For k^2-weighted EXAFS data in k-space see Figure S6c.

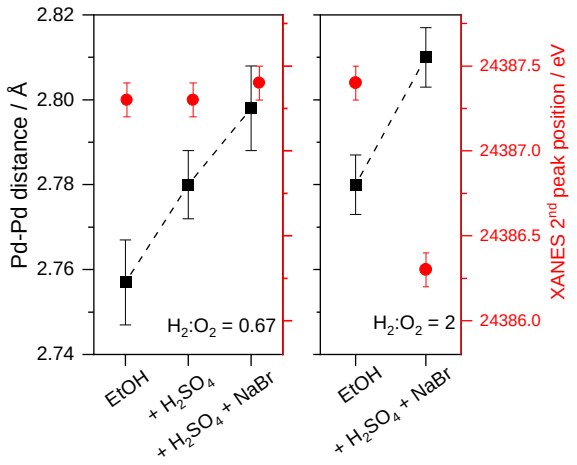

Figure 5. Average Pd-Pd distances obtained from EXAFS analysis (black squares) and position of the 2nd peak in the XANES spectra (red circles) depending on the H_2:O_2 ratio in ethanol with 0.12 M H_2SO_4 and NaBr. Dashed lines serve as guides to the eye.

Activity

Considering all operating conditions, the cerimetric redox titration indicated low H_2O_2 concentrations with a maximum of 0.40 ± 0.05 mmol/L, see Table 5. This low concentration range compared to the constant hydrogen feed concentration of 16.4 mmol/L provides an additional indicator for the differential operation mode. As a drawback of this operation mode with the low contact time, the levels of H_2O_2 observed were in the range of the limit of quantification (LDQ) of the cerimetry method. We note that the low color intensity within this H_2O_2 concentration range

did not allow using highly diluted cerium sulfate solutions for lowering the LDQ as this threshold depends on the perception of the color change. Hence, only qualitative activity trends can be drawn.

The observed H_2O_2 concentrations prove that the catalyst is active in pure ethanol and under hydrogen-rich conditions (at H_2:O_2 ratios from 1 to 2.4, Table 5). Adding sulfuric acid to ethanol results in a substantial increase in the H_2O_2 concentration by a factor of four when dosing stoichiometric amounts of hydrogen and oxygen (H_2:O_2 = 1). But the H_2O_2 productivity remains at a similar level compared to pure ethanol conditions at higher H_2:O_2 ratios of 1.5 and 2.0. No H_2O_2 was measured above this H_2:O_2 ratio within the uncertainty range. In conclusion, H_2SO_4 has a significant effect on the H_2O_2 productivity at a stoichiometric H_2:O_2 ratio with no visible effect at hydrogen excess. In contrast, no change in the H_2O_2 concentration was observed compared to acidified ethanol when further adding NaBr. Hence, addition of NaBr had no significant influence on productivity under our test conditions. It is however important to emphasize that we have assessed only the H_2O_2 productivity and did not yield the full extent of (hydrogen) conversion and selectivity. With the given low catalyst contact time in our operando study and feeding no H_2O_2, we hold the view that the measured H_2O_2 concentration strongly depends on the H_2O_2 formation rate of the parallel initial pathway (Scheme 1, pathways 1) rather than the consecutive H_2O_2-destructive pathways (Scheme 1, pathways 3 and 4). Indeed, the increase in H_2O_2 productivity we observed after acid addition at H_2:O_2 = 1 is in qualitative agreement with the results of Han, Liu and Lunsford [64,65,33]. They studied the direct synthesis with a nearly identical catalyst system (Pd/SiO_2, ethanol, various combinations of KBr, H_2SO_4 and also HCl/NaCl) operated in a semi-batch reactor with an H_2:O_2 partial pressure ratio of 0.25 (corresponding to a molar H_2:O_2 ratio in ethanol solution of about 0.1 [47]). Their experimental data show that the addition of 0.12 M H_2SO_4

to pure ethanol resulted in a 30% increase in H_2O_2 productivity [64,65]. When 0.02 mmol/L KBr was added to pure ethanol, they observed an increase in H_2O_2 selectivity of about 30% without significantly changing the H_2O_2 formation rate [33]. This is consistent with our results of adding the same amount of bromide in the form of NaBr to the acidified ethanol solution. Our findings could indicate that the promoting effect of mineral acid and bromide decreases with increasing H_2:O_2 ratio. However, to our knowledge, there is no study investigating the effect of selectivity promoters at high H_2:O_2 ratios.

The maximum H_2O_2 concentration of 0.40 ± 0.05 mmol/L in this study corresponds to a H_2O_2 productivity of 560 ± 110 $mmol_{H2O2}/(g_{Pd}\ h)$. This value is in range of productivities of most (semi-)batch experiments (500–5000 $mmol_{H2O2}/(g_{Pd}\ h)$) as summarized by Menegazzo et al. [17] (Supporting Information S7). As the catalyst also showed very little activity in our previous operando XAS study in water (Supporting Information S7), the modest H_2O_2 productivity in this study may be attributed due to the intrinsic properties of the titania-supported palladium catalyst. More precisely, the modest H_2O_2 productivity is possibly connected to the small NP size below 3 nm [27] in our experiment which is below the range of 5-15 nm preferred by Menegazzo et al. as a compromise between activity and selectivity [17]. The structure sensitivity of H_2O_2 synthesis is not studied in sufficient detail with respect to the observed accompanying hydride formation. However, hydrogenation reactions on Pd are often structure sensitive [66–68]. Different probabilities of Pd hydride phase formation for different Pd NP sizes are thought to be responsible for this structure sensitivity. This structure sensitivity is explained by simply altering the catalyst phase for larger particles while external conditions are unchanged and do not favor hydride formation for smaller NPs [66]. Therefore, we deem it important to note that larger NPs increase the probability

of PdH_x formation and, thus, we may expect different catalytic properties with potentially higher H_2O_2 productivities.

Table 5. H_2O_2 concentrations obtained in pure ethanol and with 0.12 M H_2SO_4 (addition of NaBr does not change productivities).

Conditions →		EtOH	+H_2SO_4+NaBr
No.	**H_2:O_2 ratio (-)**	**H_2O_2 concentration (mmol/L)**	**H_2O_2 concentration (mmol/L)**
1	O_2 only	< 0.05	< 0.05
2	0.67	n. a.	n. a.
3	1	0.10 (± 0.05)	0.40 (± 0.05)
4	1.5	0.05 (± 0.05)	0.10 (± 0.05)
5	2	0.10 (± 0.05)	0.05 (± 0.05)
6	2.4	0.05 (± 0.05)	< 0.05
7	3	< 0.05	< 0.05
8	H_2 only	< 0.05	< 0.05

Comparison with the previous results obtained in water as solvent

Comparing the XAS study conditions for bromide-containing water[27] and acidified ethanol containing bromide, we find a comparable low yield at a H_2:O_2 ratio of 1 of around 2% but the observed space-time yield in ethanol is increased by a factor of 25 (see Table 6). We note that in this XAS study using ethanol, the molar concentrations of dissolved H_2 and O_2 are more than three times higher compared to our previous study with water[27] but – due to the enhanced H_2/O_2 solubility in ethanol – the corresponding reactant partial pressures are even lower (Table 6). Similarly to the study in water,[27] the highest H_2O_2 concentrations in absolute ethanol were obtained in the range of H_2:O_2 ratios between 1 and 2. Under these conditions XAS identified nanoparticles with α-PdH_x structure (H_2:O_2 = 1) and a mixture of α- and β-PdH_x phases (H_2:O_2=1.5 and 2).

Unlike the study in water,[27] Pd was completely reduced by the solvent so that no PdO fingerprint could be observed in the XANES region of the spectra, and only traces of oxygen could be deduced from the contribution to the EXAFS signal (Scheme 3). Addition of H_2SO_4 and NaBr promoters to the ethanol solution led to longer Pd-Pd interatomic distances, i.e. higher fraction of β-PdH_x. At lower and stoichiometric H_2:O_2 ratios, this increased the H_2O_2 production rate assuming that decomposition and further hydrogenation of H_2O_2 are low at the given low contact time. In contrast, Pd NPs were converted to predominantly β-PdH_x under excess H_2 (H_2:O_2 = 1.5 and 2) and the obtained H_2O_2 concentration stayed the same as in absolute ethanol or even decreased. Hence, we believe that a certain mixture of α- and β-PdH_x phases is optimal for H_2O_2 formation. The promoters increase the rate of β-PdH_x formation and therefore suggest that promotors are mostly efficient below stoichiometric H_2:O_2 ratios at which otherwise only metallic Pd or only α-PdH_x phases are present. Since no spectral fingerprint of oxidized Pd^{2+} and no diminishment of Pd NP size (relatively constant Pd-Pd coordination numbers) were observed we can exclude also significant Pd leaching in form of dissolved complexes.

Table 6. Comparison of fixed bed and process metrics at H_2:O_2 = 1 for XAS studies in water[27] and ethanol.

	XAS study using water[27]	**This XAS study using ethanol**
Catalyst mass (mg)	20	35 ± 5
Palladium mass fraction (%)	1	1
Liquid feed flow (mL/min)	1.0	8.18
H_2O_2 concentration (mmol/L)	0.08	0.4 ± 0.05
H_2 and O_2 feed concentration (mmol/L)	4.8	16.4
Corresponding H_2 pressure (bar) [a]	6.0 [69]	4.8 [47]
Corresponding O_2 pressure (bar) [a]	3.4 [69]	1.7 [47]
τ_{mod} (kg_{Pd} s/m^3)	15	2.6 ± 0.4
H_2 yield (%)	1.7	2.4 ± 0.3
H_2O_2 productivity ($mmol_{H2O2}$/(g_{Pd} h))	19	560 ± 110

[a] Thermodynamic equilibrium at 293.15 K

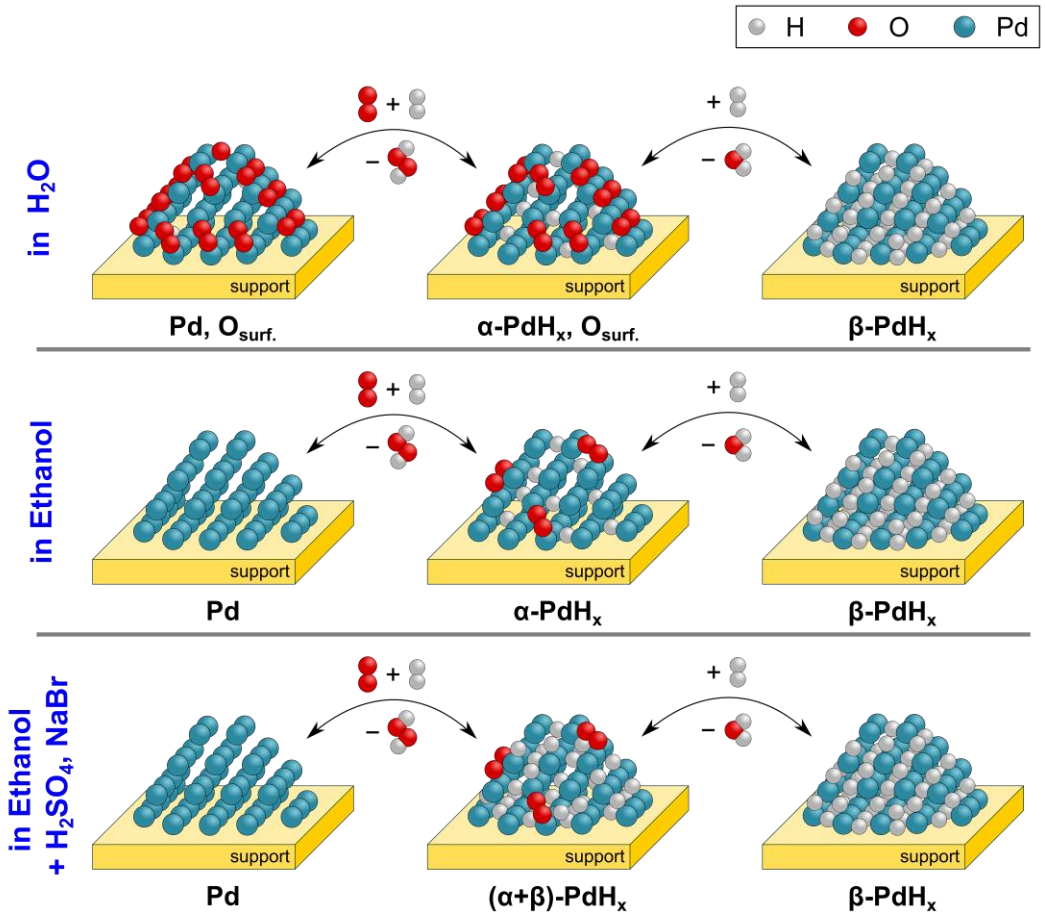

Scheme 3. Comparison of the structural data obtained during H_2O_2 synthesis in water and ethanol (this study).

Furthermore, we may speculate about the following processes that could further consolidate the existing image: In pure ethanol, the Pd NP may reduce as lattice oxygen is consumed by oxidative dehydrogenation of the solvent itself, forming adsorbed acetaldehyde and further acetate and protons. Palladium is known to convert alcohols to aldehydes at mild temperatures as low as 50°C, with the metallic phase being the active phase [71]. Moreover, acetate formation has been reported earlier via QEXAFS for flowing EtOH:H_2O (50:50 v/v) but at substantially higher temperature

(80°C) [72]. Lunsford and co-workers have speculated as early as in 2005 that acetate ions may be important in direct synthesis, modifying the Pd NP surface [65]. Spent catalyst from our experiments smelled considerably like acetic acid after a few weeks of shelf-life at room temperature, which is a further indication of this reaction path of oxidative dehydrogenation. We note that this pathway is also considered in the electrocatalytic ethanol oxidation reaction (EOR) on Pd [73]. The heterolytic mechanism with sequential proton−electron transfer (hydrogen oxidation reaction and oxygen reduction reaction; electron transport through NP lattice) proposed by Flaherty and co-workers [25] could explain the role of the solvent and the influence of the mineral acid: Without mineral acid addition, protons are delivered by amphiprotic solvent itself and the acetate-acetic acid-equilibrium at the Pd surface, limiting the overall reaction rate. Due to co-adsorbing acetate in ethanol and potentially other poisonous intermediates such as CH, CCO, C [74], the surface coverages of H and O may be altered, i.e. as observed less to no surface oxygen opposite to water. Mineral acid addition increases the H surface coverage according to the proton−electron transfer mechanism ($H^* \leftrightarrow H^+ + e^-$ [25]). This matches the observed lattice expansion as the increased surface coverage may facilitate hydride formation in turn. This contradicts a Langmuir-Hinshelwood-Hougen-Watson (LHHW) mechanism because it cannot account for the dominant role of the hydrogen availability in the lattice and solvent protons. Consequently, the well-performing mixed α/β-PdH_x may reflect a balanced, moderated hydrogen availability of Pd. A moderated hydrogen availability is already known from the selective hydrogenation of triple bonds of alkynes via Pd and Lindlar catalysts, with an α-phase being more selective but less active compared to the β-phase [75–77].

Conclusions

In this work we presented structural data on Pd NPs during H_2O_2 direct synthesis in ethanol under a broad range of parameters (H_2:O_2 ratio, addition of acidic and bromide promoters) and differential mode operation. Our study elucidates that the Pd catalyst was fully reduced upon contact with ethanol and no PdO signature could be observed in XANES. Even below stoichiometric H_2:O_2 ratios, Pd lattice expansion was observed. The lattice expansion increased at higher H_2:O_2 ratios, and increased even further as a result of adding H_2SO_4 and NaBr promoters. The highest H_2O_2 concentrations were obtained over Pd NPs with α-PdH_x structure and a mixture of α- and β-PdH_x phases, while less H_2O_2 was detected over β-$PdH_{x,}$, which could indicate that excess hydrogen of pure β-PdH_x leads to H_2O formation instead of H_2O_2 formation. In this context we propose to examine which findings from electrocatalytic reactions (e.g. the H_2O_2 electrosynthesis itself or ethanol oxidation) can be directly transferred to the direct synthesis, which would be mutually beneficial for both scientific communities. Further XAS investigations are required to obtain a comprehensive picture of the structural changes upon mineral acid addition and bromide. It would be interesting to investigate whether adding a pure acetate salt to water has the same effect as ethanol, which is thought to oxidize and in turn reduce the catalyst. Moreover, adding H_2O_2 to the feed would expand the findings to the reactor conditions at elevated conversions with a differential reactor mode. Complementary hydrogen isotope labeling the Pd NP prior to reaction could facilitate a better understanding of the Pd NP dynamics to further distinguish between the contribution of lattice hydride and protons or molecular hydrogen. As the direct synthesis can be considered as a structure-sensitive reaction, it is indispensable for a better atomistic understanding to look at the interfacial structure and Pd NP/reactant interaction under working conditions, e.g. studying the Pd NP surface coverages via operando ATR-IR spectroscopy.

Supporting Information. The following files are available free of charge. Catalyst powder characterization; H_2O_2 decomposition in the stainless-steel setup; Influence of internal mass transfer resistances; Influence of external mass transfer resistances; Near-infrared (NIR) spectra of the reactor effluent obtained during XAS measurements; EXAFS data in k-space and the quality of the corresponding fits; Comparison of H_2O_2 productivities. (PDF)

AUTHOR INFORMATION

Corresponding Author

* E-mail: benedikt.deschner@kit.edu

* E-mail: dmitry.doronkin@kit.edu

ORCID

Benedikt J. Deschner: 0000-0001-5800-7510

Dmitry E. Doronkin: 0000-0003-3930-3204

Thomas L. Sheppard: 0000-0002-8891-985X

Anna Zimina: 0000-0002-3111-7741

Jan-Dierk Grunwaldt: 0000-0003-3606-0956

Roland Dittmeyer: 0000-0002-3110-6989

Notes

The authors declare no competing financial interest.

Author Contributions

The manuscript was written through contributions of all authors. All authors have given approval to the final version of the manuscript.

ACKNOWLEDGMENT

We thank the Helmholtz Association for funding within the program Science and Technology of Nanosystems (STN). BJD and RD acknowledge funding of this work by the German Research Foundation DFG through the Research Unit 2383 “ProMiSe” (www.promise.kit.edu) under grant numbers Di 696/13-1 and Di 696/14-1. We thank Susanne Eißler for her assistance with the technical operation of the plant. We would like to thank the Institute for Beam Physics and Technology (IBPT) for the operation of the storage ring, the Karlsruhe Research Accelerator (KARA). We acknowledge Dr. Tim Prüßmann (IKFT, now INE) for his help and technical support during experiments.

REFERENCES

(1) Campos-Martin, J. M.; Blanco-Brieva, G.; Fierro, J. L. G. Hydrogen Peroxide Synthesis: An Outlook beyond the Anthraquinone Process. *Angew. Chem., Int. Ed.* **2006**, *45*, 6962–6984.
(2) Ciriminna, R.; Albanese, L.; Meneguzzo, F.; Pagliaro, M. Hydrogen Peroxide: A Key Chemical for Today's Sustainable Development. *ChemSusChem* **2016**, *9*, 3374–3381.
(3) Dittmeyer, R.; Grunwaldt, J.-D.; Pashkova, A. A Review of Catalyst Performance and Novel Reaction Engineering Concepts in Direct Synthesis of Hydrogen Peroxide. *Catal. Today* **2015**, *248*, 149–159.
(4) Huerta, I.; Biasi, P.; García-Serna, J.; Cocero, M. J.; Mikkola, J.-P.; Salmi, T. Effect of Low Hydrogen to Palladium Molar Ratios in the Direct Synthesis of H_2O_2 in Water in a Trickle Bed Reactor. *Catal. Today* **2015**, *248*, 91–100.

(5) Samanta, C.; Choudhary, V. R. Direct Formation of H_2O_2 from H_2 and O_2 and Decomposition/Hydrogenation of H_2O_2 in Aqueous Acidic Reaction Medium over Halide-Containing Pd/SiO_2 Catalytic System. *Catal. Commun.* **2007**, *8*, 2222–2228.
(6) Yook, S.; Kwon, H. C.; Kim, Y.-G.; Choi, W.; Choi, M. Significant Roles of Carbon Pore and Surface Structure in AuPd/C Catalyst for Achieving High Chemoselectivity in Direct Hydrogen Peroxide Synthesis. *ACS Sustainable Chem. Eng.* **2016**, *5*, 1208–1216.
(7) Yi, Y.; Wang, L.; Li, G.; Guo, H. A Review on Research Progress in the Direct Synthesis of Hydrogen Peroxide from Hydrogen and Oxygen: Noble-Metal Catalytic Method, Fuel-Cell Method and Plasma Method. *Catal. Sci. Technol.* **2016**, *6*, 1593–1610.
(8) Jiang, Y.; Ni, P.; Chen, C.; Lu, Y.; Yang, P.; Kong, B.; Fisher, A.; Wang, X. Selective Electrochemical H_2O_2 Production through Two-Electron Oxygen Electrochemistry. *Adv. Energy Mater.* **2018**, *8*, 1801909.
(9) Yang, S.; Verdaguer-Casadevall, A.; Arnarson, L.; Silvioli, L.; Čolić, V.; Frydendal, R.; Rossmeisl, J.; Chorkendorff, I.; Stephens, I. E. L. Toward the Decentralized Electrochemical Production of H_2O_2: A Focus on the Catalysis. *ACS Catal.* **2018**, *8*, 4064–4081.
(10) Zhou, W.; Meng, X.; Gao, J.; Alshawabkeh, A. N. Hydrogen Peroxide Generation from O_2 Electroreduction for Environmental Remediation: A State-of-the-Art Review. *Chemosphere* **2019**, *225*, 588–607.
(11) Xia, C.; Xia, Y.; Zhu, P.; Fan, L.; Wang, H. Direct Electrosynthesis of Pure Aqueous H_2O_2 Solutions up to 20% by Weight Using a Solid Electrolyte. *Science (Washington, DC, U. S.)* **2019**, *366*, 226–231.
(12) Liu, J.; He, B.; Chen, Q.; Li, J.; Xiong, Q.; Yue, G.; Zhang, X.; Yang, S.; Liu, H.; Liu, Q. H. Direct Synthesis of Hydrogen Peroxide from Plasma-Water Interactions. *Sci. Rep.* **2016**, *6*, 38454.
(13) Yi, Y.; Xu, C.; Wang, L.; Yu, J.; Zhu, Q.; Sun, S.; Tu, X.; Meng, C.; Zhang, J.; Guo, H. Selectivity Control of H_2/O_2 Plasma Reaction for Direct Synthesis of High Purity H_2O_2 with Desired Concentration. *Chem. Eng. J. (Lausanne, Switz.)* **2017**, *313*, 37–46.
(14) Flaherty, D. W. Direct Synthesis of H_2O_2 from H_2 and O_2 on Pd Catalysts: Current Understanding, Outstanding Questions, and Research Needs. *ACS Catal.* **2018**, *8*, 1520–1527.
(15) Ranganathan, S.; Sieber, V. Recent Advances in the Direct Synthesis of Hydrogen Peroxide Using Chemical Catalysis—A Review. *Catalysts* **2018**, *8*, 379.
(16) Lewis, R. J.; Hutchings, G. J. Recent Advances in the Direct Synthesis of H_2O_2. *ChemCatChem* **2019**, *11*, 298–308.
(17) Menegazzo, F.; Signoretto, M.; Ghedini, E.; Strukul, G. Looking for the "Dream Catalyst" for Hydrogen Peroxide Production from Hydrogen and Oxygen. *Catalysts* **2019**, *9*, 251.
(18) Selinsek, M.; Kraut, M.; Dittmeyer, R. Experimental Evaluation of a Membrane Micro Channel Reactor for Liquid Phase Direct Synthesis of Hydrogen Peroxide in Continuous Flow Using Nafion® Membranes for Safe Utilization of Undiluted Reactants. *Catalysts* **2018**, *8*, 556.
(19) Samanta, C. Direct Synthesis of Hydrogen Peroxide from Hydrogen and Oxygen: An Overview of Recent Developments in the Process. *Appl. Catal., A* **2008**, *350*, 133–149.
(20) Dissanayake, D. P.; Lunsford, J. H. The Direct Formation of H_2O_2 from H_2 and O_2 over Colloidal Palladium. *J. Catal.* **2003**, *214*, 113–120.
(21) Voloshin, Y.; Halder, R.; Lawal, A. Kinetics of Hydrogen Peroxide Synthesis by Direct Combination of H_2 and O_2 in a Microreactor. *Catal. Today* **2007**, *125*, 40–47.
(22) Ford, D. C.; Nilekar, A. U.; Xu, Y.; Mavrikakis, M. Partial and Complete Reduction of O_2 by Hydrogen on Transition Metal Surfaces. *Surf. Sci.* **2010**, *604*, 1565–1575.

(23) Deguchi, T.; Iwamoto, M. Catalytic Properties of Surface Sites on Pd Clusters for Direct H_2O_2 Synthesis from H_2 and O_2: A DFT Study. *J. Phys. Chem. C* **2013**, *117*, 18540–18548.
(24) Wang, G.; Yao, R.; Xin, H.; Guan, Y.; Wu, P.; Li, X. At Room Temperature in Water: Efficient Hydrogenation of Furfural to Furfuryl Alcohol with a Pt/SiC–C Catalyst. *RSC Adv.* **2018**, *8*, 37243–37253.
(25) Wilson, N. M.; Flaherty, D. W. Mechanism for the Direct Synthesis of H_2O_2 on Pd Clusters: Heterolytic Reaction Pathways at the Liquid-Solid Interface. *J. Am. Chem. Soc.* **2016**, *138*, 574–586.
(26) Ledendecker, M.; Pizzutilo, E.; Malta, G.; Fortunato, G. V.; Mayrhofer, K. J. J.; Hutchings, G. J.; Freakley, S. J. Isolated Pd Sites as Selective Catalysts for Electrochemical and Direct Hydrogen Peroxide Synthesis. *ACS Catal.* **2020**, *10*, 5928–5938.
(27) Selinsek, M.; Deschner, B. J.; Doronkin, D. E.; Sheppard, T. L.; Grunwaldt, J.-D.; Dittmeyer, R. Revealing the Structure and Mechanism of Palladium during Direct Synthesis of Hydrogen Peroxide in Continuous Flow Using Operando Spectroscopy. *ACS Catal.* **2018**, *8*, 2546–2557.
(28) Kanungo, S.; van Haandel, L.; Hensen, E. J.; Schouten, J. C.; Neira d'Angelo, M. F. Direct Synthesis of H_2O_2 in AuPd Coated Micro Channels: An In-Situ X-Ray Absorption Spectroscopic Study. *J. Catal.* **2019**, *370*, 200–209.
(29) Biasi, P.; Mikkola, J.-P.; Sterchele, S.; Salmi, T.; Gemo, N.; Shchukarev, A.; Centomo, P.; Zecca, M.; Canu, P.; Rautio, A.-R. et al. Revealing the Role of Bromide in the H_2O_2 Direct Synthesis with the Catalyst Wet Pretreatment Method (CWPM). *AIChE J.* **2017**, *63*, 32–42.
(30) Lunsford, J. H. The Direct Formation of H_2O_2 from H_2 and O_2 over Palladium Catalysts. *J. Catal.* **2003**, *216*, 455–460.
(31) Choudhary, V.; Samanta, C. Role of Chloride or Bromide Anions and Protons for Promoting the Selective Oxidation of H_2 by O_2 to H_2O_2 over Supported Pd Catalysts in an Aqueous Medium. *J. Catal.* **2006**, *238*, 28–38.
(32) Burch, R.; Ellis, P. R. An Investigation of Alternative Catalytic Approaches for the Direct Synthesis of Hydrogen Peroxide from Hydrogen and Oxygen. *Appl. Catal., B* **2003**, *42*, 203–211.
(33) Liu, Q.; Lunsford, J. H. Controlling Factors in the Direct Formation of H_2O_2 from H_2 and O_2 over a Pd/SiO_2 Catalyst in Ethanol. *Appl. Catal., A* **2006**, *314*, 94–100.
(34) Biasi, P.; Canu, P.; Menegazzo, F.; Pinna, F.; Salmi, T. O. Direct Synthesis of Hydrogen Peroxide in a Trickle Bed Reactor: Comparison of Pd-Based Catalysts. *Ind. Eng. Chem. Res.* **2012**, *51*, 8883–8890.
(35) Gemo, N.; Salmi, T.; Biasi, P. The Use of Modelling to Understand the Mechanism of Hydrogen Peroxide Direct Synthesis from Batch, Semibatch and Continuous Reactor Points of View. *React. Chem. Eng.* **2016**, *1*, 300–312.
(36) Grunwaldt, J.-D.; Baiker, A. Time-Resolved and Operando XAS Studies on Heterogeneous Catalysts — From the Gas Phase Towards Reactions in Supercritical Fluids. *AIP Conf. Proc.* **2007**, *882*, 577–581.
(37) Rehr, J. J.; Albers, R. C. Theoretical Approaches to X-ray Absorption Fine Structure. *Rev. Mod. Phys.* **2000**, *72*, 621–654.
(38) Centomo, P.; Meneghini, C.; Zecca, M. Versatile Plug Flow Catalytic Cell for In Situ Transmission/Fluorescence X-ray Absorption Fine Structure Measurements. *Rev. Sci. Instrum.* **2013**, *84*, 54102.

(39) Centomo, P.; Meneghini, C.; Sterchele, S.; Trapananti, A.; Aquilanti, G.; Zecca, M. EXAFS In Situ: The Effect of Bromide on Pd during the Catalytic Direct Synthesis of Hydrogen Peroxide. *Catal. Today* **2015**, *248*, 138–141.
(40) Centomo, P.; Meneghini, C.; Sterchele, S.; Trapananti, A.; Aquilanti, G.; Zecca, M. In Situ X-ray Absorption Fine Structure Spectroscopy of a Palladium Catalyst for the Direct Synthesis of Hydrogen Peroxide: Leaching and Reduction of the Metal Phase in the Presence of Bromide Ions. *ChemCatChem* **2015**, *7*, 3712–3718.
(41) Kanungo, S.; Paunovic, V.; Schouten, J. C.; Neira d'Angelo, M. F. Facile Synthesis of Catalytic AuPd Nanoparticles within Capillary Microreactors Using Polyelectrolyte Multilayers for the Direct Synthesis of H_2O_2. *Nano Lett.* **2017**, *17*, 6481–6486.
(42) Doronkin, D. E.; Wang, S.; Sharapa, D. I.; Deschner, B. J.; Sheppard, T. L.; Zimina, A.; Studt, F.; Dittmeyer, R.; Behrens, S.; Grunwaldt, J.-D. Dynamic Structural Changes of Supported Pd, PdSn, and PdIn Nanoparticles during Continuous Flow High Pressure Direct H_2O_2 Synthesis. *Catal. Sci. Technol.* **2020**, *10*, 4726–4742.
(43) Rueter, M.; Zhou, B.; Parasher, S. Process for Direct Catalytic Hydrogen Peroxide Production. U. S. Patent 7144565, July 23, 2004.
(44) Desmedt, F.; Miquel, P.; Vlasselaer, Y. Direct Synthesis of Hydrogen Peroxide. WO Patent 2014072169, October 22, 2013.
(45) Inoue, T.; Schmidt, M. A.; Jensen, K. F. Microfabricated Multiphase Reactors for the Direct Synthesis of Hydrogen Peroxide from Hydrogen and Oxygen. *Ind. Eng. Chem. Res.* **2007**, *46*, 1153–1160.
(46) Solvay Chemicals, Inc. Passivation of Laboratory Equipment for Hydrogen Peroxide Service: Technical Data Sheet. http://hydrogen-peroxide.us/chemical-handling-toxicity/Solvay-Hydrogen-Peroxide-Lab-Eq-passivation-2004.pdf (accessed January 7, 2019).
(47) Luehring, P.; Schumpe, A. Gas Solubilities (Hydrogen, Helium, Nitrogen, Carbon Monoxide, Oxygen, Argon, Carbon Dioxide) in Organic Liquids at 293.2 K. *J. Chem. Eng. Data* **1989**, *34*, 250–252.
(48) DIN 1343:1990-01, Reference Conditions, Normal Conditions, Normal Volume: Concepts and Values; German Version January 1990; Beuth: Berlin, 1990.
(49) Pinho, S. P.; Macedo, E. A. Solubility of NaCl, NaBr, and KCl in Water, Methanol, Ethanol, and Their Mixed Solvents. *J. Chem. Eng. Data* **2005**, *50*, 29–32.
(50) Ojeda Toro, J. C.; Dobrosz-Gómez, I.; Gómez García, M. Á. Sodium Sulfate Solubility in (Water+Ethanol) Mixed Solvents in the Presence of Hydrochloric Acid: Experimental Measurements and Modeling. *Fluid Phase Equilib.* **2014**, *384*, 106–113.
(51) Devic, M.; Delais, L. Method for Preparing an Aqueous Hydrogen Peroxide Solution Directly from Hydrogen and Oxygen. U. S. Patent 6447742, September 8, 2000.
(52) Weisz, P. B.; Prater, C. D. In *Advances in Catalysis*; Frankenburg, W. G., Komarewsky, V. I., Rideal, E. K., Eds.; Academic: New York, 1954; Vol. 6, pp 143–196.
(53) Mears, D. E. Tests for Transport Limitations in Experimental Catalytic Reactors. *Ind. Eng. Chem. Process Des. Dev.* **1971**, *10*, 541–547.
(54) Zimina, A.; Dardenne, K.; Denecke, M. A.; Doronkin, D. E.; Huttel, E.; Lichtenberg, H.; Mangold, S.; Pruessmann, T.; Rothe, J.; Spangenberg, T. et al. CAT-ACT—A New Highly Versatile X-ray Spectroscopy Beamline for Catalysis and Radionuclide Science at the KIT Synchrotron Light Facility ANKA. *Rev. Sci. Instrum.* **2017**, *88*, 113113.
(55) Ravel, B.; Newville, M. ATHENA, ARTEMIS, HEPHAESTUS: Data Analysis for X-ray Absorption Spectroscopy using IFEFFIT. *J. Synchrotron Radiat.* **2005**, *12*, 537–541.

(56) Bugaev, A. L.; Guda, A. A.; Lomachenko, K. A.; Srabionyan, V. V.; Bugaev, L. A.; Soldatov, A. V.; Lamberti, C.; Dmitriev, V. P.; van Bokhoven, J. A. Temperature- and Pressure-Dependent Hydrogen Concentration in Supported PdH_x Nanoparticles by Pd K-Edge X-ray Absorption Spectroscopy. *J. Phys. Chem. C* **2014**, *118*, 10416–10423.
(57) Lengeler, B. Lattice Site Location of Hydrogen by Use of Extended X-Ray Absorption Fine Structure. *Phys. Rev. Lett.* **1984**, *53*, 74–77.
(58) Wang, J.; Wang, Q.; Jiang, X.; Liu, Z.; Yang, W.; Frenkel, A. I. Determination of Nanoparticle Size by Measuring the Metal–Metal Bond Length: The Case of Palladium Hydride. *J. Phys. Chem. C* **2015**, *119*, 854–861.
(59) Akiba, H.; Kobayashi, H.; Kitagawa, H.; Kofu, M.; Yamamuro, O. Glass Transition and Positional Ordering of Hydrogen in Bulk and Nanocrystalline Palladium. *Phys. Rev. B* **2015**, *92*, 189.
(60) Bugaev, A. L.; Guda, A. A.; Lomachenko, K. A.; Shapovalov, V. V.; Lazzarini, A.; Vitillo, J. G.; Bugaev, L. A.; Groppo, E.; Pellegrini, R.; Soldatov, A. V. et al. Core–Shell Structure of Palladium Hydride Nanoparticles Revealed by Combined X-ray Absorption Spectroscopy and X-ray Diffraction. *J. Phys. Chem. C* **2017**, *121*, 18202–18213.
(61) Manchester, F. D.; San-Martin, A.; Pitre, J. M. The H-Pd (Hydrogen-Palladium) System. *J. Phase Equilib.* **1994**, *15*, 62–83.
(62) Yamauchi, M.; Ikeda, R.; Kitagawa, H.; Takata, M. Nanosize Effects on Hydrogen Storage in Palladium. *J. Phys. Chem. C* **2008**, *112*, 3294–3299.
(63) Johansson, M.; Skúlason, E.; Nielsen, G.; Murphy, S.; Nielsen, R. M.; Chorkendorff, I. Hydrogen Adsorption on Palladium and Palladium Hydride at 1 bar. *Surf. Sci.* **2010**, *604*, 718–729.
(64) Han, Y.-F.; Lunsford, J. H. A Comparison of Ethanol and Water as the Liquid Phase in the Direct Formation of H_2O_2 from H_2 and O_2 over a Palladium Catalyst. *Catal. Lett.* **2005**, *99*, 13–19.
(65) Han, Y.-F.; Lunsford, J. H. Direct Formation of H_2O_2 from H_2 and O_2 over a Pd/SiO_2 Catalyst: The Roles of the Acid and the Liquid Phase. *J. Catal.* **2005**, *230*, 313–316.
(66) Karpiński, Z. In *Advances in Catalysis*; Eley, D. D., Pines, H., Weisz, P. B., Eds.; Academic Press: New York, 1990; Vol. 37, pp 45–100.
(67) Semagina, N.; Renken, A.; Laub, D.; Kiwi-Minsker, L. Synthesis of Monodispersed Palladium Nanoparticles to Study Structure Sensitivity of Solvent-Free Selective Hydrogenation of 2-Methyl-3-butyn-2-ol. *J. Catal.* **2007**, *246*, 308–314.
(68) Carturan, G. Hydrogenation of Nitrocompounds with Supported Palladium Catalysts: Influence of Metal Dispersion and Nitrocompound Nature. *J. Catal.* **1983**, *82*, 56–65.
(69) Sander, R. Compilation of Henry's Law Constants (Version 4.0) for Water as Solvent. *Atmos. Chem. Phys.* **2015**, *15*, 4399–4981.
(70) Battino, R.; Rettich, T. R.; Tominaga, T. The Solubility of Nitrogen and Air in Liquids. *J. Phys. Chem. Ref. Data* **1984**, *13*, 563–600.
(71) Grunwaldt, J.-D.; Caravati, M.; Baiker, A. Oxidic or Metallic Palladium: Which is the Active Phase in Pd-Catalyzed Aerobic Alcohol Oxidation? *J. Phys. Chem. B* **2006**, *110*, 25586–25589.
(72) Newton, M. A.; Brazier, J. B.; Barreiro, E. M.; Parry, S.; Emmerich, H.; Adrio, L. A.; Mulligan, C. J.; Hellgardt, K.; Hii, K. K. Operando XAFS of Supported Pd Nanoparticles in Flowing Ethanol/Water Mixtures: Implications for Catalysis. *Green Chem.* **2016**, *18*, 406–411.

(73) Krittayavathananon, A.; Duangdangchote, S.; Pannopard, P.; Chanlek, N.; Sathyamoorthi, S.; Limtrakul, J.; Sawangphruk, M. Elucidating the Unexpected Electrocatalytic Activity of Nanoscale PdO Layers on Pd Electrocatalysts towards Ethanol Oxidation in a Basic Solution. *Sustainable Energy Fuels* **2020**, *4*, 1118–1125.
(74) Wu, Z.-P.; Miao, B.; Hopkins, E.; Park, K.; Chen, Y.; Jiang, H.; Zhang, M.; Zhong, C.-J.; Wang, L. Poisonous Species in Complete Ethanol Oxidation Reaction on Palladium Catalysts. *J. Phys. Chem. C* **2019**, *123*, 20853–20868.
(75) Albers, P. W.; Möbus, K.; Frost, C. D.; Parker, S. F. Characterization of β-Palladium Hydride Formation in the Lindlar Catalyst and in Carbon-Supported Palladium. *J. Phys. Chem. C* **2011**, *115*, 24485–24493.
(76) Albers, P.; Pietsch, J.; Parker, S. F. Poisoning and Deactivation of Palladium Catalysts. *J. Mol. Catal. A: Chem.* **2001**, *173*, 275–286.
(77) Palczewska, W. In *Advances in Catalysis*; Eley, D. D., Pines, H., Weisz, P. B., Eds.; Academic Press: New York, 1975; Vol. 24, pp 245–291.

TOC Image